

### 4.3 Realistic site response estimation and tsunami synthesis in the Catania area

(F. Romanelli, F. Vaccari and G. F. Panza)

Using the modal summation technique, extended to laterally heterogeneous anelastic structural models (Vaccari *et al.*, 1989; Romanelli *et al.*, 1996), a database of synthetic signals has been generated, which can be used for the study of the local response at a set of selected sites, located within the Catania area (Fig. 4.8). To minimize the number of free parameters Romanelli and Vaccari (1999) decided to account for source finiteness by properly weighting the point source spectrum using the scaling laws of Gusev (1983), as reported in Aki (1987). The used focal mechanism parameters of the source (latitude: 37.44°; longitude: 15.23°), are: strike=352°, dip= 0°, rake=270°, focal depth=10 km and seismic moment=3.5·10<sup>19</sup> Nm.

The same source model has been adopted for the generation of synthetic mareograms at three selected sites in Eastern Sicily (Fig. 4.8), using the efficient algorithm (Panza *et al.*, 1999) that represents the direct extension of the modal summation technique, valid for Rayleigh waves, to the Tsunami mode propagating in laterally varying oceanic models.

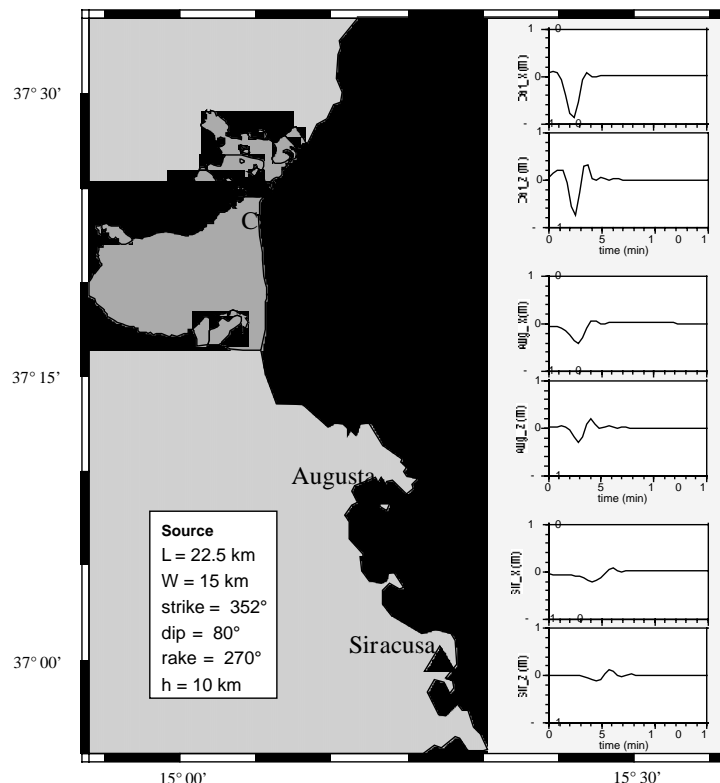


Figure 4.8 - Schematic view of the Catania area and the position of the considered fault model. The star indicates the location of the earthquake point source. On the right are shown the synthetic Tsunami signals, radial (x) and vertical (z) component, calculated at Catania (Cat), Augusta (Aug) and Siracusa (Sir); the ordinates are in m.

### 4.3.1 Site response estimation in the Catania area

For the definition of the structural model, Romanelli and Vaccari (1999) used the geotechnical information collected within the Catania Project (Faccioli, 1997), that is, a simplified geotechnical zonation map and a set of five detailed geotechnical cross-sections. Since the modal summation technique can be applied both to rough and detailed laterally heterogeneous models, the previous authors first employed the simplified map, to analyze the effects of the gross features of the geotechnical zonation on the ground motion. As a second step, in order to test the usefulness of the simplified models, they considered a detailed version of one of the cross-sections.

In figure 4.9 the simplified geotechnical zonation map for the Catania area, together with the 13 cross-sections considered in the analysis, are shown. Along each section, a set of sites is considered; the site locations are chosen both in the proximity of the boreholes, and at the edges of the section. The laterally varying models associated with each cross-section are built up by putting in welded contact (from 2 to 4) different 1-D local models; the regional model, assigned to Eastern Sicily (Costa *et al.*, 1993), is chosen as the bedrock model and the geotechnical information related to the selected boreholes are used for the definition of the local models.

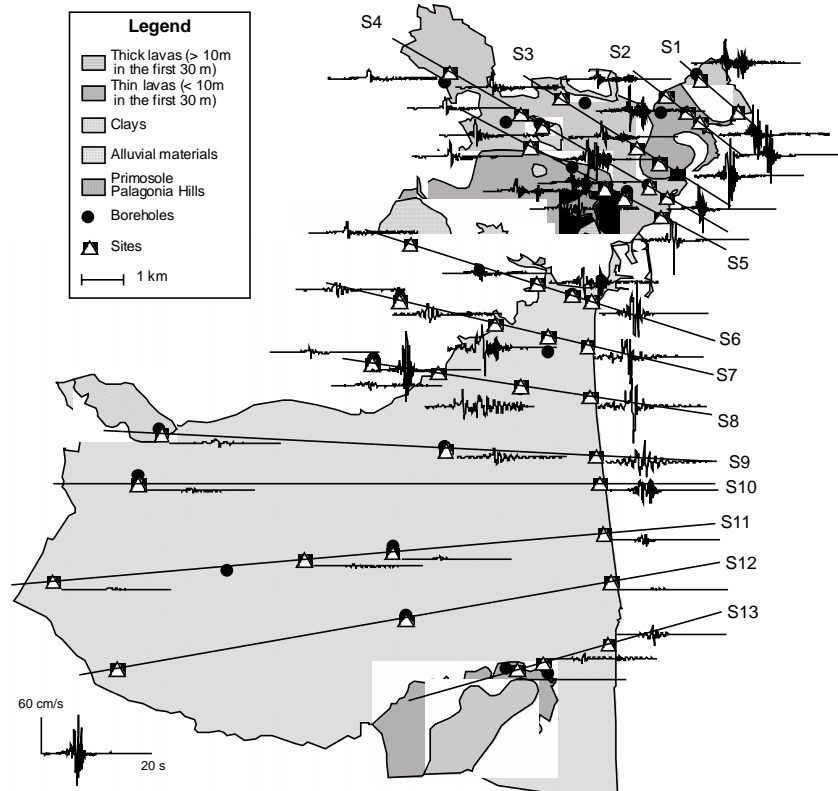


Figure 4.9 - Simplified geotechnical zonation map for the Catania area and the first 20 s of the velocities time series (SH motion), calculated at the sites. Each signal is scaled to the maximum value of  $V_{MAX}$  (63 cm/s) over the entire area (black triangle) (modified from Romanelli and Vaccari, 1999).

The map shown in figure 4.9 defines the borders between the local models, i.e. the distances between the vertical interfaces separating the different 1-D models. In figure 4.9 the synthetic velocity time series (SH motion) calculated at the considered sites are shown. The cut-off frequency of the signals is 10 Hz, but their spectra show that most of the energy is concentrated at frequencies below 4 Hz. Each record is 20 s long and is normalized to the peak velocity value (63.1 cm/s), VMAX, for the entire region.

Since for cross-section S10 detailed geotechnical information is available (Faccioli, 1997), we can compare the results obtained using the simplified laterally heterogeneous model with those obtained for a realistic model of a geological cross-section. The detailed laterally heterogeneous model, used for the calculation of the synthetic seismograms along S10, is built up using forty-eight local models in welded contact, for a total extension of approximately 13 km (Fig. 4.10). The source is buried in the regional bedrock model. The spectral analysis of the signals shown in Figure 4.9, indicate that a reasonable upper frequency limit for the detailed calculations can be 4 Hz. The signals are calculated for a set of sites, one for each local model, along the section. We give an estimation of the local response at each site, evaluating the response spectra ratio, RSR, corresponding to the laterally varying model and to the bedrock model.

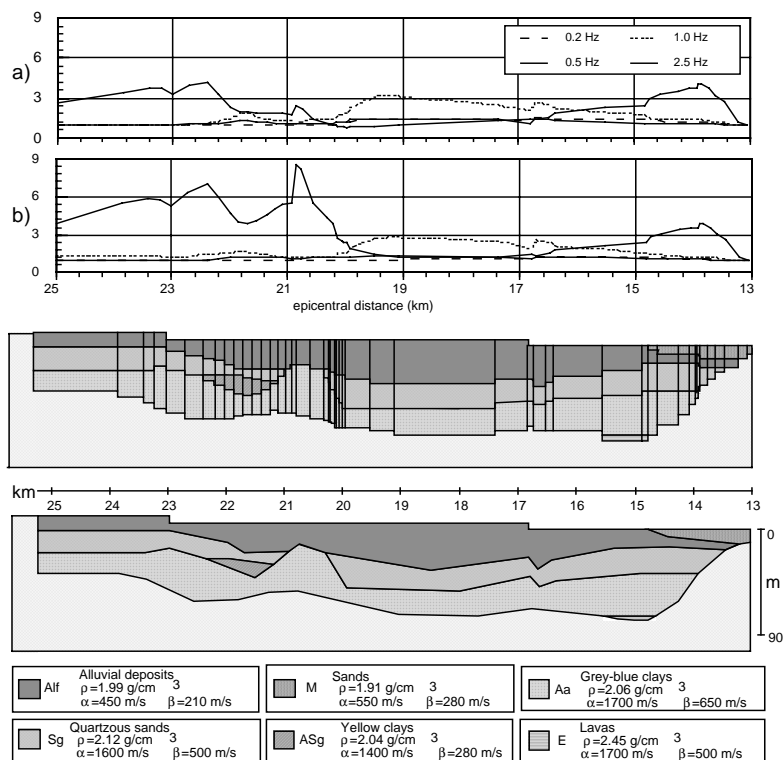


Figure 4.10 - Cross-section (bottom) and corresponding model for cross-section S10. The distance along the section is measured in km from the source, while the vertical scale is in m. a) Response spectra ratio at four selected frequencies (0.2 Hz, 0.5 Hz, 1.0 Hz, 2.5 Hz) versus epicentral distance, for the transverse component of motion; strike-section angle equal to 80°. b) Same as a) but the strike-section angle is equal to 180°.

Figure 4.10 (a,b) shows the variation of the RSR (SH motion) along the profile: part a) shows the RSR at four selected frequencies (0.2, 0.5, 1.0, 2.5 Hz) and it is obtained using the signals calculated with a strike-section angle equal to  $80^\circ$ ; part b) is obtained for a value of the angle between the fault strike and the cross-section equal to  $180^\circ$ , that corresponds to a maximum of the SH radiation pattern in the direction of the cross-section. As expected, at low frequencies (0.2 - 0.5 Hz) the ratios are approximately 1 all along the section, but at higher frequencies the wavelengths are comparable to the dimensions of the lateral heterogeneities, and the local effects become important. The shape of the curves corresponding to 2.5 Hz seems to resemble the sub-surface topography of the Alf and Aa layers respectively.

In figure 4.11 the RSR, for SH motion, versus the epicentral distance and frequency are shown for strike-section angles equal to  $80^\circ$  and  $180^\circ$ , respectively. Along the first part of the section the amplification pattern is quite simple, but for distances larger than 20 km the amplification level changes significantly with distance and frequency. This example shows that the interference between seismic waves and the lateral heterogeneities is azimuthally dependent and may therefore be responsible for different responses at the same site. Such a result should cast some doubts both on the convolutional representation and on the validity of local soil effects determinations made with very popular methods that do not consider the realistic propagation and interference of seismic waves (an experimental evidence can be found e.g. in Wang and Nisimura, 1999).

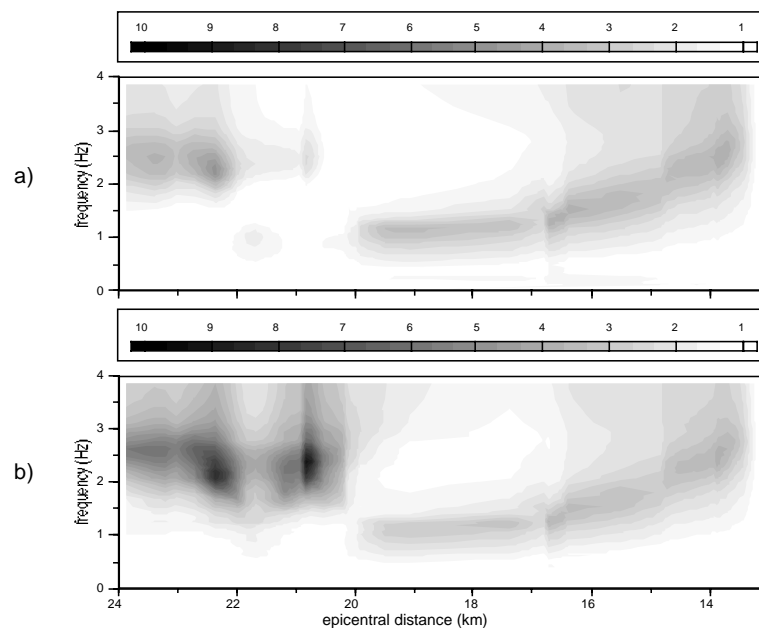


Figure 4.11 - a) RSR versus epicentral distance and versus frequency for SH motion; strike-section angle equal to  $80^\circ$ . b) Same as a) but the strike-section angle is equal to  $180^\circ$  (from Romanelli and Vaccari, 1999).

The results obtained for the detailed model of cross-section S10 can easily be compared with those coming from the simplified model at the corresponding sites. A

set of 48 synthetic signals, filtered with a cut-off frequency of 4 Hz, is calculated along S10, using the simplified laterally heterogeneous model shown in Figure 4.12b. In Figure 4.12a the RSR are shown, versus epicentral distance and frequency, for the strike-section angle equal to  $80^\circ$  using the simplified model. The RSR corresponding to the simplified model have a very sharp discontinuity close to the beginning of the local model at an epicentral distance of 13 km. This discontinuity is responsible for the excitation of high frequency diffracted waves that are rapidly decaying with increasing distance from the boundary. Away from the boundary, the pattern becomes relatively simple: the greatest amplifications are obtained around the frequency of 1.5 Hz, that is the value of the fundamental resonant frequency for the stack of local layers shown in the left part of Figure 4.12b. The results summarized in Figures 4.11 and 4.12 show that the extension of punctual information to extended cross-sections, i.e. the adoption of simplified models, could lead to misleading conclusions concerning the seismic response of sedimentary basins.

The RSR obtained using the synthetic signals calculated for the P-SV motion along the detailed cross-section S10, are shown versus epicentral distance and frequency in Figure 4.13. The strike-section angle is  $80^\circ$ , a value that, for the given focal mechanism, corresponds approximately to a maximum in the radiation pattern for the P-SV waves. For epicentral distances less than about 20 km the pattern of the resonance frequencies shown in Figure 4.13a (radial component) resembles the pattern visible in Figure 4.10a and b.

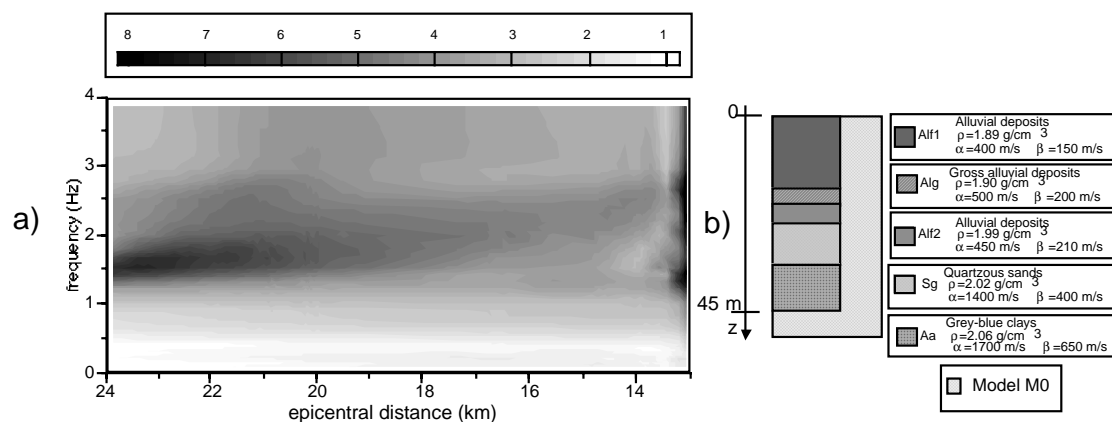


Figure 4.12 - a) RSR obtained for the simplified laterally heterogeneous models of section S10 for SH motion. The RSR are plotted versus the epicentral distance and versus frequency for the strike-section angle equal to  $80^\circ$ ; b) Simplified model of S10 constructed from the geotechnical map shown in Figure 4.9.

Figure 4.12b shows that, in this case, the vertical component of motion is not much affected by the local geological conditions. In Figure 4.13c the H/V RSR are shown versus epicentral distance and frequency. The calculations confirm the empirical conclusions that the resonance patterns are very well correlated with surface geology, but the absolute level of amplification cannot be straightforwardly determined (e.g. Lachet and Bard, 1994).

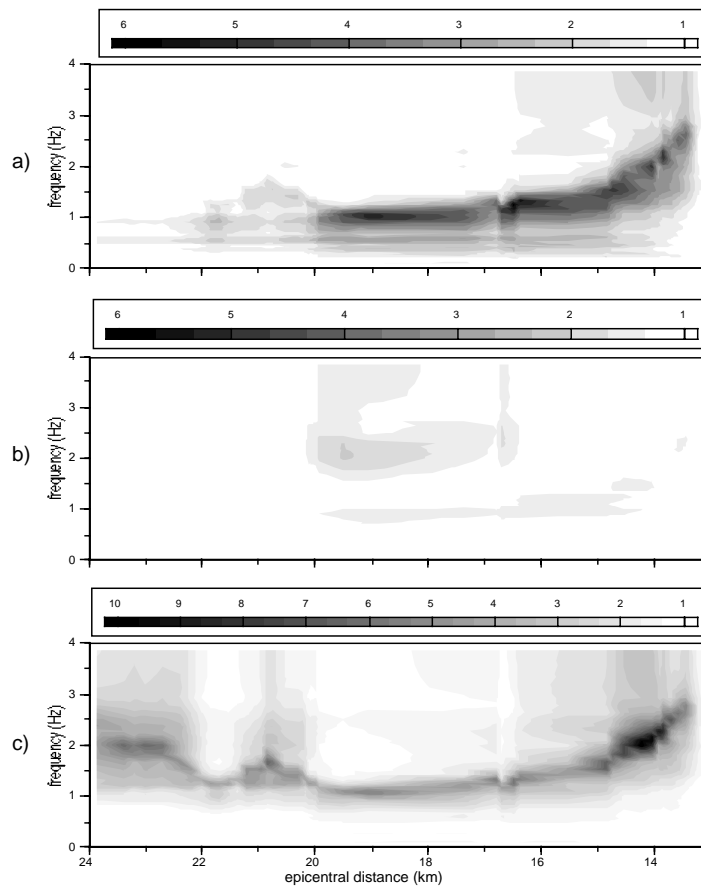


Figure 4.13 - a) RSR for the radial component of motion versus epicentral distance and frequency; b) RSRs for the vertical component of motion versus epicentral distance and frequency; c) H/V RSR versus epicentral distance and frequency. Strike-section angle equal to  $80^\circ$  (from Romanelli and Vaccari, 1999). The gray scale in part c) is different from the ones in parts a) and b).

#### 4.3.2 Evaluation of the damage potential of the synthetic signals

The synthetic signal database, generated as shown in the previous sub-section, can be used as seismic input in a subsequent engineering analysis, at a very low cost/benefit ratio. For the estimation of the destructive potential of some of the signals calculated for the simplified geological models, some parameters, obtained from: (a) direct analysis, (b) integration in the time or in the frequency domain, and (c) the structural (elastic and anelastic) response, have been investigated by Decanini et al. (1999). The synthetic signals, for the transverse component of motion (SH problem), were calculated at a series of equally spaced sites along Section 4 (see Figure 4.9). The distance between each site is 200 m and the total number of computed signals is 20: 15 are calculated on the local model M1 (lavas) and 5 on M2 (sands and clays).

On the basis of the parameters characterizing the earthquake destructiveness power, derived from the available strong motion records, the results of Decanini et al. (1999) show that the synthetic signals provide an energy response which is typical of accelerograms recorded on intermediate-firm soil, at a distance from the causative fault between 12 km and 30 km, and a magnitude between 6.5 and 7.1. Figure 4.14 shows a comparison between the elastic input energy of three synthetic signals (synth\_1, synth\_3 and synth\_5), evaluated for a damping ratio equal to 5%, and two accelerograms (Santa Cruz UCSC/Lick Obs. Elect. Lab., Uscs0; and Gilroy # 1, Gavilan College, Water Tower, Gav. Tower 90) recorded during the Loma Prieta earthquake (1989,  $M=7.1$ ) on firm soil (S1) and at distances from the surface projection of the causative fault ( $D_f$ ) equal to 15 and 16 km, respectively. It can be observed that the frequency content is almost the same in both cases, and the maximum values of  $E_I$  are concentrated within the range of periods  $0.3 \leq T \leq 0.5$  s. Therefore, distances from the causative fault being equal, the synthetic signals provide an elastic energy comparable to that obtained from records taken on firm soil for a magnitude approximately equal to 7.1.

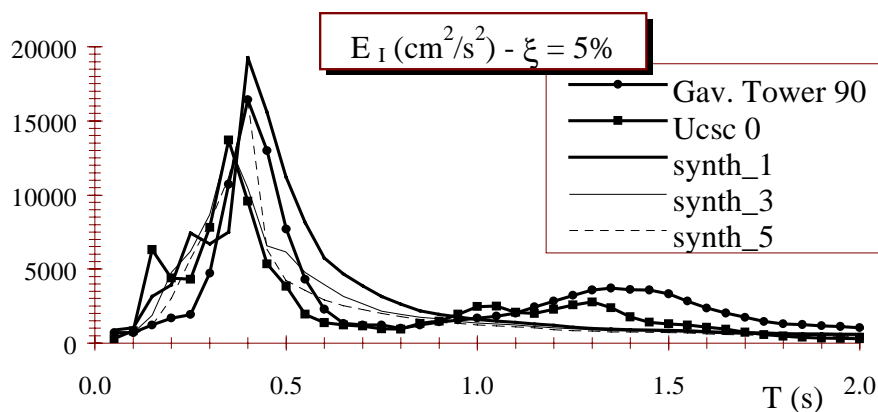


Figure 4.14 - Elastic  $E_I$  ( $\text{cm}^2/\text{s}^2$ ) spectra. Comparison between synthetic signals and strong motion records of Loma Prieta earthquake (1989), Soil S1 (from Decanini et al., 1999).

### 4.3.3 Examples of Tsunami synthesis in the Catania area

We studied how the tsunami mode is generated by a scaled double-couple seismic source and how it propagates in realistic oceanic models (Fig.4.8). The method developed and used in this work is the direct extension to tsunami waves, propagating in multilayered oceanic media, of the well-known multimodal method (e.g. Haskell, 1953), which has been successfully employed for the study of Rayleigh waves in multilayered structures and for the construction of broad-band synthetic seismograms (e.g. Panza, 1985). We solve the equations of elastic motion when a constant gravitational field acts in the downward direction in the multilayered fluid which is in sliding contact with a multilayered solid half-space where we assume that

only elastic forces act. In such a way we can use the efficient algorithms valid for flat, multilayered oceanic structures, for the production of synthetic mareograms due to the excitation, by seismic sources, of the tsunami mode propagating in oceanic structures. This method is then extended to laterally heterogeneous structures in order to study the effect of the variation of the ocean bottom. The increase of the tsunami wavetrain maximum amplitude in shallow water is caused not only by the conservation of the energy flux for a given frequency and then a distribution of the flux over a thinner water layer, but also by the decrease of the velocity dispersion at the frequencies corresponding to the maximum radiation. This method has been applied for the Tsunami synthesis, adopting the same source model described in subsection 4.3.1, at the sites of Catania, Augusta and Siracusa (Fig.4.8), allowing, in a very efficient way, to estimate the maximum expected height for an event similar to the 1693 one.